Chemical and temporal manipulation of early steps in protein assembly tunes the structure and intermolecular interactions of protein-based materials

Valeria Italia, Amanda Jons, Bhavika Kaparthi, Britt Faulk, Marco Maccarini, Paolo Bertoncello, Ken Meissner, Donald Martin, Sarah Bondos

▶ **To cite this version:**

Valeria Italia, Amanda Jons, Bhavika Kaparthi, Britt Faulk, Marco Maccarini, et al.. Chemical and temporal manipulation of early steps in protein assembly tunes the structure and intermolecular interactions of protein-based materials. Protein Science, 2025, 34 (2), pp.e70000. ⟨10.1002/pro.70000⟩. ⟨hal-04906512⟩

HAL Id: hal-04906512

https://hal.science/hal-04906512v1

Submitted on 27 Jul 2025

HAL is a multi-disciplinary open access archive for the deposit and dissemination of scientific research documents, whether they are published or not. The documents may come from teaching and research institutions in France or abroad, or from public or private research centers.

L'archive ouverte pluridisciplinaire **HAL**, est destinée au dépôt et à la diffusion de documents scientifiques de niveau recherche, publiés ou non, émanant des établissements d'enseignement et de recherche français ou étrangers, des laboratoires publics ou privés.

HAL Authorization

Chemical and temporal manipulation of early steps in protein assembly tune the structure and intermolecular interactions of protein-based materials

V. Italia1; A. Jons2,3; B. Kaparthi2; B. Faulk4,5 ; M. Maccarini6, P. Bertoncello7 K. Meissner1; D. K. Martin6 ; S. E. Bondos2,3,4

1Department of Physics, Swansea University, Swansea, UK
2Department of Cell Biology and Genetics, Texas A&M Health Science Center, Texas A&M University, Bryan, Texas, USA 3Interdisciplinary Graduate Program in Genetics, Texas A&M University, College Station, Texas, USA
4Department of Medical Physiology, School of Medicine, Texas A&M University, Bryan, Texas, USA
5Department of Biochemistry and Biophysics, Texas A&M University, College Station, Texas, USA
6University Grenoble Alpes, SyNaBi, TIMC-IMAG/CNRS/INSERM, UMR 5525, Grenoble, France
7Department of Chemical Engineering, Swansea University, Swansea, UK

Abstract

Protein-based materials have numerous potential applications, especially in tissue engineering and medical devices. These advances require a variety of biomaterials, each with specific morphologies, properties, and functions. Most new biopolymers are created by changing the composition of the monomers or the method used to drive assembly. In contrast, in this study we used the same monomers and assembly approach while altering the assembly time and chemical environment to generate materials with different morphologies and intermolecular interactions. This is possible because the protein assembly process primarily relies on noncovalent interactions, which are extremely sensitive to their environment. When assembled using standard conditions, the *Drosophila* protein Ultrabithorax (Ubx) undergoes a hierarchical, multi-step assembly process, forming linear arrays of monomers which pack laterally into fibrils and films. We analysed the impact of protein concentration, assembly time, and subphase composition on Ubx assembly using Langmuir experiments. In low salt buffers, we generated a new type of Ubx material using 5-fold less protein, and 100-fold less assembly time. Ubx monomers in these new materials appear randomly arranged in films and exhibit more dityrosine covalent cross-links per monomer. These covalent bonds do not require the same tyrosines necessary for crosslinking previously established Ubx materials. Differences in monomer packing and crosslinking also alter the extent of wrinkling on the fiber surface. A new image analysis technique based on autocorrelation of Scanning Electron Microscopy (SEM) images was developed to quantify these structural differences. We conclude that varying the assembly conditions represents a facile and inexpensive process for creating new materials. Since many proteins can undergo multi-step, multi-scale self-assembly processes, this approach should be applicable to other protein systems.

Keywords: protein-based materials, monomer packing, crosslinking, Langmuir films, dityrosine, chemical environment

1. Introduction

Inspired by biology, methods have been developed to create synthetic protein-based materials *in vitro* for many applications, including drug delivery, tissue engineering, biosensors, cell culture studies and biomedical devices[1-3]. Each application requires the materials to have the appropriate topology, mechanical properties, and/or porosity for timely chemical / ligand diffusion[2-5]. These properties are all determined by the structure of the biomaterial. In turn, the

 © xxxx IOP Publishing Ltd

materials' structure is determined by the mechanism through which the protein monomers self-assemble.

Ubx self-assembles in a series of defined steps [8,9,14-17]. The early steps are unlikely to involve a large number of

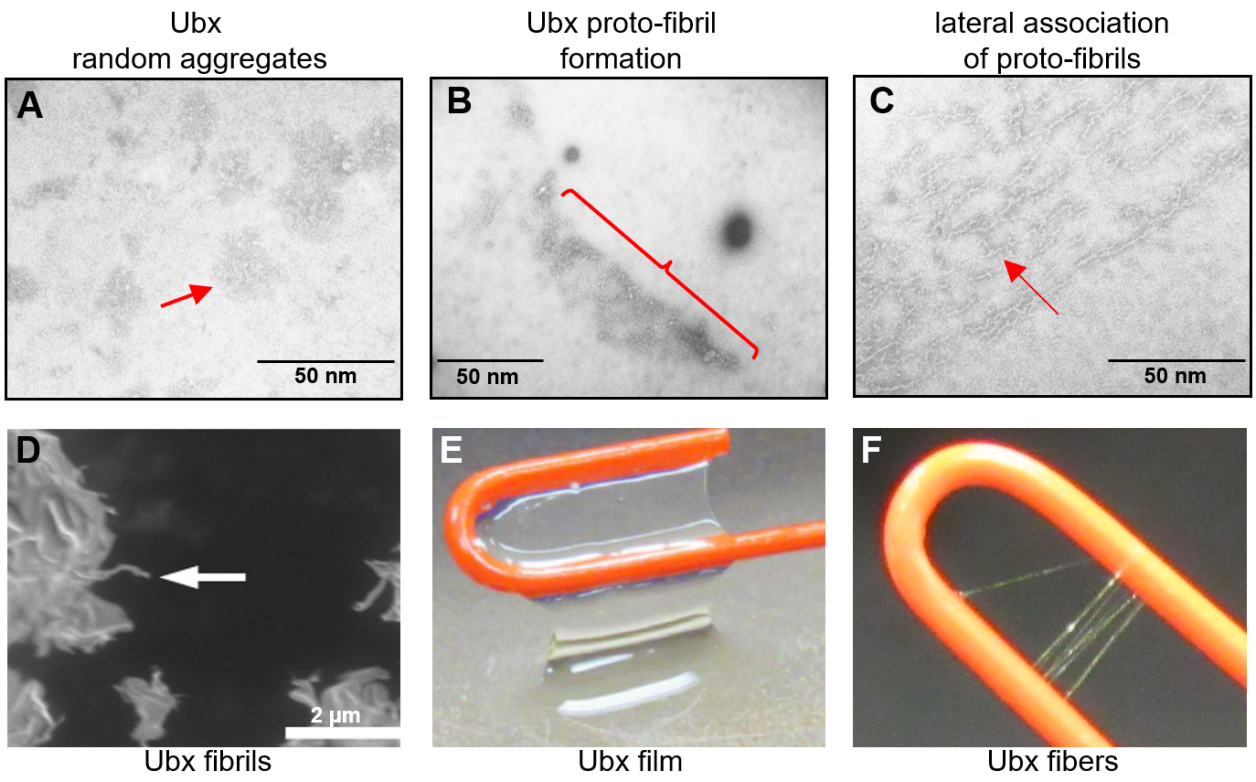

Figure 1. *Hierarchical assembly of Ubx materials. (A) About 15min after dilution into a tray, Ubx begins to form irregular aggregates (red arrow). (B) Within 1h, these aggregates begin to spontaneously reshape into lines of Ubx proteins, termed protofibrils. (C) After 1h, the protofibrils align in parallel and begin to form side-to-side contacts. (D) After 1-2h multiple protofibrils condense to form fibrils about 50 nm in diameter (white arrow). Fibrils also interact laterally to form films which can be lifted from the surface (E). Alternately, films on the air–water interface can be drawn into fibers composed of aligned fibrils (F). (A–C) 100-nm thick carbon films were placed on the surface of the Ubx solution, lifted using TEM grids, stained with 2% w/v phosphotungstic acid and imaged by TEM. (D) A film was transferred to a metal stub, sputter coated in gold, and imaged by scanning electron microscopy. Panels (A)–(C): Reprinted from reference 8 with permission. Panel (D): Panels A-D reprinted from references 8 and 14 with permission.*

Several proteins, including Collagen, various silks, Mussel Adhesive Protein, and Ultrabithorax (Ubx), have the ability to self-assemble at the air-water interface, forming a film that can be re-arranged into other shapes[6-12]. Film-formation is the rate-limiting step that establishes many of the intermolecular interactions, and thus the properties, of the final material[11,12]. The initial steps of film formation rely on interactions between monomers, and between monomers and aggregates. Because these interactions are non-covalent, they are very sensitive to the environment[12,13]. Consequently, the chemical and physical conditions present during these early steps has the potential to impact the assembly kinetics, monomer interactions/packing and the structure, behavior, and yield of the final macroscale materials.

To investigate such environmental influences on material formation, we selected the *Drosophila melanogaster* Hox transcription factor Ultrabithorax (Ubx), as a model monomer. intermolecular covalent bonds because we have been unable to detect blue fluorescence from these bonds at this stage, and because monomer intermolecular contacts significantly rearrange during assembly. Therefore, these steps have the potential to be influenced by their environment. We also used monomers composed of Ubx that was genetically fused to Enhanced Green Fluorescent Protein (EGFP)[16]. The resulting fusion protein is termed EGFP-Ubx. In the EGFP-Ubx amino acid sequence, the last amino acid of EGFP and the first amino acid of Ubx are both covalently bound to a short amino acid linker via peptide bonds. Ubx and EGFP-Ubx monomers spontaneously self-assemble *ex vivo* at an air-water interface to form biopolymeric materials (Figure 1)[14]. During this hierarchical, multistep process, Ubx monomers first form nanoscopic aggregates, which then reorganize to create lines of protein monomers, termed protofibrils[8]. Lateral association of protofibrils generates fibrils with a diameter similar to

amyloid fibrils, although not amyloid in structure[14]. Fibrils associate laterally to form a macroscale thin film, which can either be used as is or drawn into biocompatible fibers[9]. The properties of the film determine the properties of the resulting fibers: fiber diameter, which ranges from 2 – 400 μm, depends on the thickness of the film, whereas the surface area of the film determines fiber length, which can reach several meters[15,18,19].

Here we investigated the early stages of Ubx assembly using Langmuir surface adsorption experiments, which measures phenomena that occur at an air-water interface[20]. By varying protein concentration, subphase properties and assembly times, we discovered a protocol to prolong the lifetime of films composed of randomly packed Ubx, an obligatory early intermediate in the Ubx assembly process (New Figure 1A). By stabilizing this state, we could draw these early films into fibers, which were compared with Ubx fibers produced under standard conditions. Different tyrosine residues participate in forming dityrosine covalent cross-links than in transitional fibers, confirming that Ubx is differently packed in these novel materials. These bonds lock the protein monomers into a randomly packed configuration, ultimately affecting the surface structure of the resulting fibers. A new image analysis technique based on autocorrelation of Scanning Electron Microscopy (SEM) images was developed to quantify these structural differences. These new materials, formed using the same monomers and surface assembly/compression technique, exhibit more than 3-fold more crosslinks per monomer than traditional fibers, and require 5-fold-less protein and 100-fold less assembly time to form.

2. Methods

1.1 EGFP-Ubx protein Expression and Purification

Following previously described techniques, the EGFP-Ubx fusion protein was cloned into the pET19b vector (Novagen) and transformed into Rosetta(DE3)pLysS *E. coli* cells (Novagen)[8,18,21]. Cells were cultured overnight in Luria Broth containing 50 μg/mL ampicillin and 30 μg/mL chloramphenicol, at 37°C. *E. coli* cell culture (8 mL) was used to inoculate 1 L of Luria Broth media which was fermented until reaching an optical density at 600 nm between 0.6 and 0.8. EGFP-Ubx protein expression was then induced with 1 mM isopropyl b-D-1-thiogalactopyranoside (IPTG) at 26°C prior to another overnight fermentation. Cells were harvested using 30 minutes of centrifugation at 4°C. The collected pellet was stored at -20°C.

Each pellet was lysed in 40 mL of lysis buffer (50 mM sodium phosphate buffer, pH=8.0, 5% glucose w/v, 500 mM NaCl, 1 Roche Complete Mini Protease Inhibitor Cocktail tablet, 0.8 mg/L DNase I) for 20 minutes and centrifuged at 4°C for 30 minutes. The supernatant was loaded in a 10 mL nickel−nitrilotriacetic acid (Ni-NTA) agarose resin column (Fisher), that was previously equilibrated with 50 mL of buffer G0 (50 mM sodium phosphate buffer, pH=8.0, 5% glucose w/v, 500 mM NaCl). The column was iteratively washed with 10 column volumes of buffer G0 containing 0, 20, 40 and 80 mM imidazole. The purified proteins were eluted with 25 mL of buffer G0 containing 300 mM Imidazole and stored at -20°C.

The concentration of EGFP-Ubx proteins was calculated from the absorbance of EGFP using the Lambert-Beer law and an extinction coefficient of 56 $(mM\ cm)^{-1}$ at 488 nm[22,23].

1.2 Generation of EGFP-Ubx Fibers

Fibers were collected from the Langmuir tray or the "buffer reservoir" tray using a 10 μL sterile plastic inoculation loop with the handle cut away as previously described[18]. The loop was touched gently on the surface of the buffer and moved away to pull the fiber from the EGFP-Ubx surface film. Since the film is composed of nanoscale fibrils, withdrawing the plastic loop slowly allows a microscale fiber to be drawn from the surface film and wrapped around the loop which acts as a support. The resulting fiber-wrapped loop was immobilized in a sterile plastic petri dish to slowly dehydrate the fibers, and stored at room temperature until use.

1.3 Scanning Electron Microscopy (SEM)

SEM images were recorded with a Hitachi S4800 FE-SEM operating at V = 1 kV and I = 5 μA. The samples were fixed to a specimen holder (SEMClip, 32 x 10mm, M4 cylinder mount, 2 clips from Agar Scientific). To obtain a uniform image without noise, we also used double-sided carbon tape to further stabilize the sample. No coating was needed for the fibers since Ubx-based materials are weakly conductive.

1.4 Image analysis

The assessment of the alignment and uniformity of the wrinkle components was done with an in-house developed MATLAB code. An axial autocorrelation was employed to identify large scale continuity in structural features (e.g.. wrinkles, on the surface of the fibers. The full width at half of the maximum height (FWHM) of the resulting graph was used to quantify the long-range alignment. The FWHM is correlated with long range order. If the wrinkles are well ordered, they stay aligned during the axial autocorrelation, creating a wide FWHM. If the wrinkles are randomly distributed, the alignment would deteriorate quickly during the axial autocorrelation creating a narrow FWHM. Therefore, the FWHM of the autocorrelation trace is a measure of the fiber structure with a larger FWHM indicating long-range ordered structure to the fiber.

A continuous wavelet transform using a standard Morse basis wavelet was used to visualize the spatial periodicity across the

wrinkles. This analysis can detect local repeated patterns that may not extend through the length of the fiber. To increase the signal to noise ratio, the pixel intensities were averaged over a 0.1 μm longitudinal section of the fiber. The results are displayed in a color-coded scalogram where a higher magnitude (more yellow) indicates a strong relation of that frequency around that area of the fiber. In addition, by looking at which frequencies are present in the signal, the approximate size of the wrinkles can be determined by taking the inverse of the frequency (Figure 3).

1.5 Langmuir Technique and Limiting Area Analysis

Our protocols are based on previous studies on Bovine Serum Albumin (BSA)[20], which has a molecular weight similar to that of EGFP-Ubx. The measurements of π-A isotherms were carried out on a KSV NIMA Langmuir Large KN2003 (PTFE; total area 841 cm^2) equipped with a dipping well and a dipping mechanism. All solutions and buffers were prepared using deionized water purified using a Mili-Q (18 mΩ·cm) purification system. The Langmuir trough was cleaned prior to use with warm water and acetone to remove any trace contaminants. The trough was filled with water or saline solution as indicated. With the barriers fully open, specified amounts of stock spreading solution (purified EGFP-Ubx protein diluted to 10 mM in purified water) was added to the subphase surface using the microspreading technique[24,25], in which small drops of protein were added directly and symmetrically across the surface of the trough. Proteins were allowed to equilibrate for varying times, as indicated, before beginning barrier compression at a rate of 25 cm^2/min and at room temperature. The π-A isotherms of Ubx proteins were measured to investigate the effects of three critical parameters: concentration of EGFP-Ubx; buffer in which EGFP-Ubx is dissolved and assembly time after protein introduction. A minimum of 3 replicates were completed for each condition. In each panel, data were collected with the same protein preparation and on the same day to avoid the influence of weather on laboratory environmental conditions and, hence, materials assembly. Unlike water insoluble molecules like lipids, proteins such as Ubx are partially soluble in water. Thus, some fraction of the protein added to the surface will dissolve in the subphase. Consequently, the x-axis of the pressure-area isotherms is reported as cm^2 instead of nm^2/molecule, a standard practice for experiments involving soluble proteins[26]. The limiting area was calculated by extrapolating the linear part of the curve to the x-axis[27-30].

1.6 Confocal Microscopy

Confocal microscopy was used to compare the density of blue-fluorescent dityrosine bonds in Ubx materials formed under different conditions. In EGFP-Ubx fibers, the green fluorescence provided by the EGFP component correlated with the density of protein within the materials and was used to normalize the dityrosine data. Since fibers have different sizes, the fluorescence intensity was also normalized to fiber diameter. In this way we compared measurements derived from different samples[20,31].

Fiber samples were collected for confocal microscopy analysis from different trays in which the buffer, protein concentration, and incubation time were varied. As indicated, some fibers were assembled using a low protein concentration in a 100 mM NaCl buffer (a condition termed "pb" herein) while other fibers were assembled using a high protein concentration in buffer G0 (PB condition). Buffer G0 contains 5% glucose w/v, 500 mM NaCl, 50 mM sodium phosphate buffer, pH=8.0. Fibers were collected after either a 10-minute incubation time or an overnight incubation for each condition. Fibers were air-dried overnight before being imaged with a Nikon Eclipse Ti A1R inverted confocal microscope equipped with NIS Elements AR 4.10.01 software to analyse fluorescent intensity of both the DAPI (488 nm) and FITC (405 nm) channels. All data were averaged from at least 3 separate fibers, and each fiber was measured 3 independent times. Thus, each LA value reflects a minimum of 9 measurements. Microscope settings were constant, and all images were taken with a 20x objective using the FITC channel at a gain of 52 and DAPI channel at a gain of 120.

3. Results

3.1 Fiber Structure

The discovery of films composed of randomly packed protein aggregates provides an opportunity to try to draw fibers from these films and compare their structure and composition with that of standard Ubx fibers drawn from aligned films. Surprisingly, films constructed using low amounts of protein and a brief 10-minute incubation of EGFP-Ubx, could still produce fibers. Because the films were small and thin compared to films formed later during assembly, the fibers were also thinner and more difficult to lift from the film surface. Using 2 nmol plain Ubx protein over buffer G0, we compared fibers generated after 10, 60, or 120 minutes assembly time. These parameters coincide with the different stage of assembly in our prior electron microscopy experiments (Figure 1).

The surfaces of the resulting fibers are different (Figure 2). As films are drawn into fibers, folds in the film create wrinkles visible on the fiber surface. Films exhibiting irregular edges have difficulty merging into a single, gap-free structure as the surface is compressed. Such films produce fibers with visible discontinuities, appearing as pits or unaligned wrinkles on the surface. While fibers created after a 10-minute incubation present some pits and knobs, the visible wrinkles are mostly aligned. Fibers obtained after waiting 60 minutes, during which the film reorganizes, display a non-continuous and winding pattern of wrinkles. We suspect that the lack of long-range order in the fibers reflects the lack of long range order

and the small, discontinuous shape of the films. Finally, fibers obtained after an ordered, linear film has formed at 120 minutes incubation have deep, aligned wrinkles. Deeper appear as a spike embedded in a short cone, and thus have a very small width at half height. Because the lines depicted in panel A are oriented in the same direction as the movement of

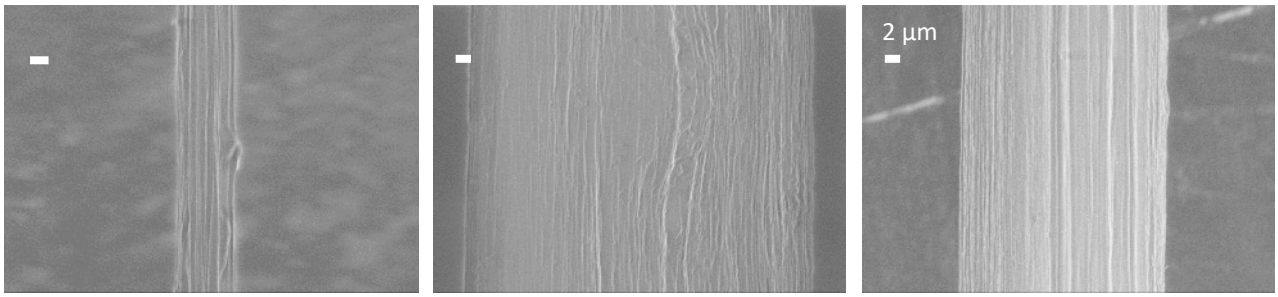

Figure 2. *Fibers drawn from a Langmuir trough with 2 nmol Ubx in buffer G0 and assembling for left) 10 minutes, yielding a fiber diameter of 4.5 ± 1.0 µm, center) 60 minutes to generate a fiber with a diameter of 43 ± 3 µm and right) 120 minutes (26 µm ± 2 µm diameter fiber) were imaged using a Scanning Electron Microscope with 1 kV voltage. These diameters reflect the film thickness and the density of protein within the film.*

wrinkles and larger folds are consistently created from films that are thicker and/or more highly crosslinked. Thus, there is a clear correlation between the properties of the surface film and the nature of the fibers drawn from that film.

To quantify these observations, we used both autocorrelation and wavelet analysis. Autocorrelation analysis evaluates the extent of overlap as one image is moved vertically across another. An example of a perfectly autocorrelated sample is a series of parallel straight lines (Figure 3A). Imagine placing two copies of this image, one above the other, and then sliding the top image down across the other image. Before the images overlap, aspects of the image (white vs. black) do not overlap, and the y-axis value is 0. When the parallel lines in the image first begin to overlap, signal is generated when any black pixels overlap other black pixels, or white overlaps white. The more the images overlap, the larger percentage of each line is in register and the higher the value of the y-axis in the autocorrelation graph. When the image and its copy are perfectly aligned, then all points on one image correlate with its copy on the other image and the y-axis value is 1. As the images then begin to move apart, the auto-correlation decreases, a reverse of the prior process. If a random image is subjected to this same analysis, then the only correlation observed as the images begin to overlap would occur by random chance as light or dark pixels happen to overlap. This random level of correlation would occur less frequently, but would increase as the images overlap to a greater extent, because there are more opportunities for two overlaid pixels to have the same coloration. Thus, on the autocorrelation graph, the lines to either side of X = 0 have a steeper slope. When the two random images overlay perfectly (Vertical Translation Position is 0), suddenly all points are correlated, yielding a spike of height 1. Thus, the autocorrelation graph of a well-correlated image will appear like a cone and have a large width at half the maximum height (red line in Figure 3B), whereas a poorly correlated image will the image, all of the lines (or, in our analysis, wrinkles) do not need to be the same width to be well correlated. The top and bottom of a consistently wide wrinkle will still correlate, as will the top and bottom of a thin wrinkle.

Autocorrelation graphs for Ubx fibers formed from films incubated for 10, 60, or 120 minutes are shown in Figure 3D-F, respectively. Fibers drawn after allowing film to form for 10 minutes yielded an autocorrelation graph in which the full width at half maximum height (FWHM) was 4.34 µm. As expected, autocorrelation analysis of the 60-minute fibers yields a smaller FWHM = 2.48 µm, indicating a more disorganized surface. This disorganization of the fiber surface originates from the 60-minute films, indicating that these films were not as well-packed as the films present at 10 minutes. This poor packing is consistent with disassembly of the initial randomly organized film (Figure 1B), which has not yet reorganized. Finally, fibers generated from film incubated for 120 minutes, which has had the opportunity to re-organize into laterally interacting linear aggregates, exhibited the most organization, with a significant increase in the structural linearity and continuity (FWHM = 8.72 µm).

The autocorrelation data determines the extent to which large features (here, wrinkles) persist over long distances (10s of µm) in the fibers. In other words, is a wrinkle that is wide the top of the microscopy image still wide at the bottom of that same image? To identify repetitive features that persist over smaller distances, a wavelet analysis was performed across a 0.1 µm horizontal slice across each fiber. The advantage of the wavelet analysis is that the analysis can identify changes in spatially repeating structures across the fiber. In other

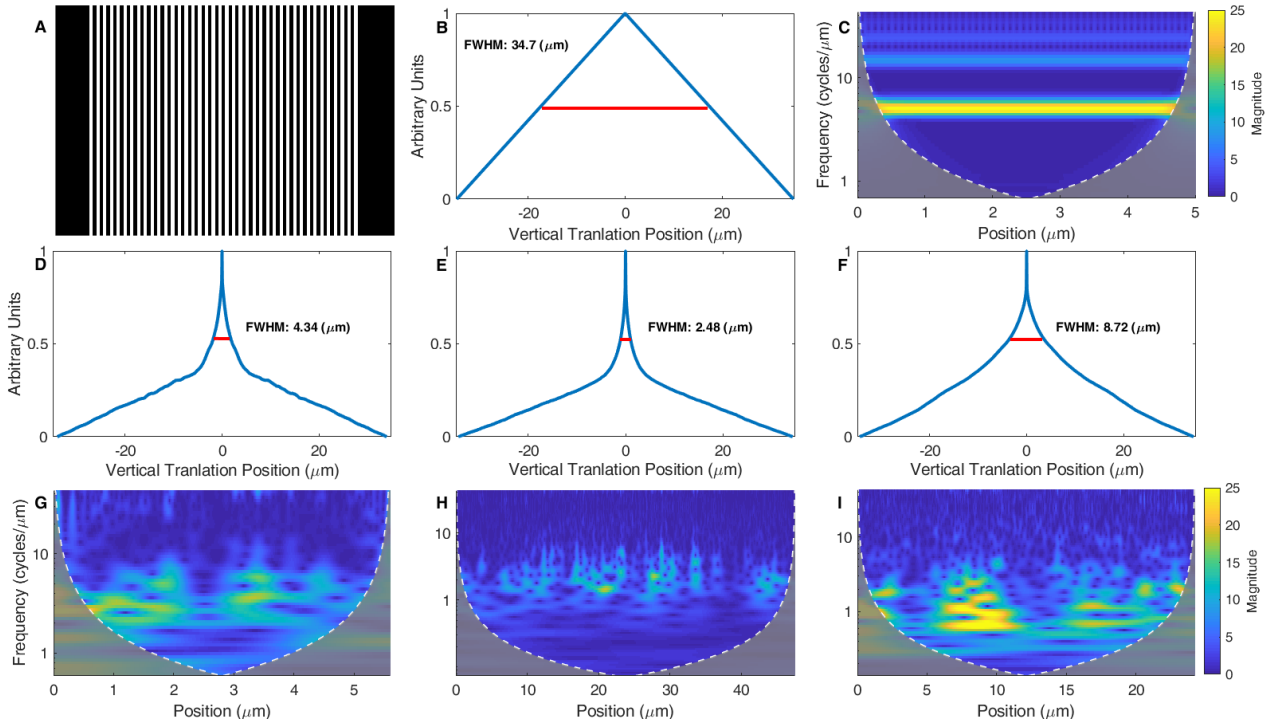

Figure 3. *Ideal case of perfectly aligned fibers (A) and the corresponding autocorrelation (B) and wavelet analysis (C). Autocorrelation from representative fibers with 10 (D), 60 (E), and 120 (F) minutes of wait time prior to starting the compression of the Langmuir trough. The FWHM is marked by the red line and the value is provided aside the line. Wavelet analysis of the fibers reveals lateral uniformity and wrinkle sizes for assembly times of 10 (G), 60 (H), and 120 minutes (I).*

words, is a wide wrinkle likely to be adjacent to other wide wrinkles, creating a repeating pattern? If so, in what region of the fiber is this pattern observed?

Like a Fourier analysis, a wavelet analysis looks for spatial frequencies, in cycles per distance, within the fiber. A range of frequencies (vertical axis) are tested to determine how well they match the image, and where within the image / slice the match occurs. This method creates a spectrogram in which the vertical axis is the spatial frequency of the structure. The horizontal axis is the distance across the fiber and the color identifies the magnitude of the spatial frequency at each point on the fiber where the analysis is run. The resulting "U-shaped" data starts at the spatial frequency matching the entire the width of the fiber (the bottom of the y-axis) and, therefore, only produces one data point positioned at the center of the fiber. As the spatial frequency increases (moving up the vertical axis), the frequency repeats more times across the sample and the number of data points corresponding to that frequency increases.

In the fiber formed after a 10-minute waiting period (Fig. 3G), structure (generally wrinkles) with spatial frequencies around a few cycles/μm are identified, as shown by the yellow/green areas on the spectrogram. While some wrinkles are observed across most of the width of the fiber, these structural features are less regular (only green intensity) and only persists for 0.25 – 0.5 μm across the fiber. In the fiber formed after a 60-minute waiting time (Fig. 3H), a much smaller fraction of the fiber has surface features and the signal from these features is not as strong. Thus, any wrinkles present lose any semblance of a consistent size or periodicity. In contrast, for the fiber formed after a 120-minute waiting time (Fig. 3I), the wrinkles persist across the width of the fiber (green signal). Around 10 μm this signal strengthens (yellow), reflecting well-repeating structures. The repeating structures persist for ~5 μm across the fiber, a long distance relative to the size of Ubx monomer (~5 nm). The analysis clearly shows that the 120-minute fiber displays the most regular structural features, followed by the 10-minute fiber. The 60-minute fiber has a very irregular surface.

These SEM images and analysis by autocorrelation and wavelet experiments demonstrate that the films produced after different incubation times produce fibers with different surface characteristics. It follows that the films that produced these fibers also have different structures. In particular, after 120 minutes of incubation, organized linear arrays of Ubx have formed and had enough time to interact with each other, interact and rotate to minimize gaps, and create larger, more robust films that produce fibers with pronounced, regular wrinkles on the surface. Importantly, wrinkling impacts the

ability of cells to attach and migrate on a surface[32,33]. Therefore, techniques that alter the presence, depth, and consistency of wrinkles on the surface of materials may alter cell: material interactions as well.

3.2 Langmuir film formation

we observed film formation using the Langmuir technique, which is the premier approach to measure assembly in two dimensions at the air-water interface. In a Langmuir trough, a protein is added to the surface of a subphase liquid, and then the protein is allowed to interact with itself and the air/water interface for a set period of time. Following this incubation,

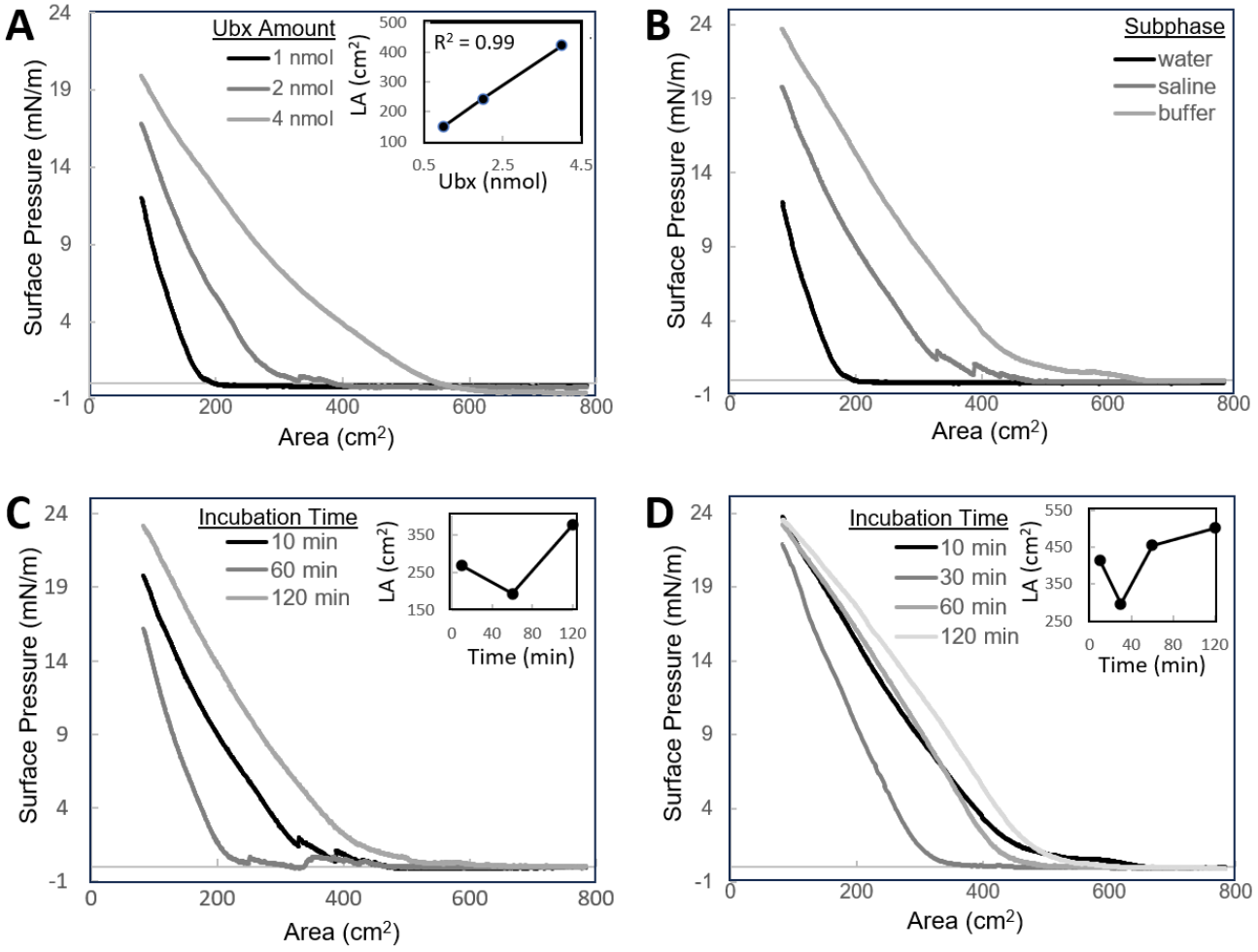

Figure 4. *Isothermal compression curves of EGFP-Ubx. A) 10-minute assembly times, 100 mM NaCl buffer at different protein concentrations. B) 10-minute assembly times, 2 nmol protein in different buffers. C) 2 nmol EGFP-Ubx with different assembly times in 100 mM NaCl solution. D) 2 nmol EGFP-Ubx with different assembly times in 100 mM NaCl+ 0.05 M NaH_2PO_4 pH= 8.0 subphase. Bumps in these curves that occur before (to the right of) the gas-liquid transition have been attributed to rotation of long, thin islands of films, allowing them to pack in parallel as the surface is compressed.*

We hypothesized that differences observed in the surface of the fibers are caused by changes in the packing of monomers at the film stage. Indeed, prior microscopy experiments suggested that Ubx self-assembles into a random film, then disassembles that structure and reassembles into a new film composed of linear arrays of Ubx (Figure 1). However, these samples had to be manipulated to move them from the surface of a liquid to a form compatible with electron microscopy. To ensure that these differences in monomer packing within films was not an artifact of sample preparation, the surface area is reduced by contraction of two movable barriers. As protein aggregates come into contact, phase transitions in the Langmuir film are produced[34]. At the start of the procedure (the lower right side of the pressure-area graphs in Figure 4), the available area per molecule is large, and so the proteins do not interact with each other. This portion of the experiment is termed the “gas phase”. Compressing the monolayer forces the proteins to become more closely packed and commence interactions with each other, creating the “liquid phase”. For Ubx, which forms small films – like

islands – of aggregates, the liquid phase begins when small, isolated films are forced into proximity. When the proteins are close to their maximum packing, they have reached the "solid phase", and any further compression would cause the film to wrinkle or fold over itself[35,36]. Since we are interested in studying the early phases of Ubx assembly, the transition from the gas phase to the liquid phase is of primary interest.

To observe such early phases of assembly, the Langmuir technique generally requires pure water or low salt concentrations in the subphase. The high surface tension of water helps to reduce the interparticle distance between large molecules or colloids deposited on the surface, thus promoting assembly[37]. The addition of salts and sugars to the subphase can further increase the surface tension, potentially driving the system into the liquid or solid phase before compression begins, which would prevent observation of these transitions[38,39].

Previously established conditions were optimized to drive Ubx self-assembly. Typically, 15 nmol of Ubx was spread across a 338 cm^2 surface in which the subphase is a high salt buffer (0.5 M NaCl, 0.05 M NaH_2PO_4, 5% w/v D-Glucose pH=8.0)[40]. To slow Ubx association and allow us to measure discrete early stages of assembly, we reduced both the amount of protein utilized and the concentration of salts and glucose in the buffer.

These experiments used a fusion protein in which Enhanced Green Fluorescent Protein is covalently attached, via a peptide bond, to a short linker peptide which, in turn, is fused via another peptide bond to the N-terminus of Ubx, creating EGFP-Ubx[16] (Supplemental Figure 1). Ubx and EGFP-Ubx self-assemble into materials equally well[16,41].

To characterize EGFP-Ubx monomer oligomerization and biopolymeric film formation obtained under different conditions, we used a Langmuir trough to obtain surface pressure–area (π-A) isotherms[42-44]. The shape of the isotherm depends on the shape and area occupied by the aggregates, which, in turn, depends on nature of the amphiphile (herein, EGFP-Ubx), the compression speed, the spreading conditions, the temperature, and the time allowed for protein assembly prior to barrier compression. To identify appropriate parameters for these experiments, the first tests varied the amount of EGFP-Ubx monomers added to identify conditions under which we can best observe the gas phase to liquid phase transition[20] (Figure 4A). These experiments used 100 mM NaCl solution in the subphase and 10-minute assembly time prior to compression. This assembly time was selected to catch the earliest stage of Ubx assembly, based on our prior electron microscopy data (Figure 1). We tested adding 1, 2, or 4 nmol of EGFP-Ubx to the trough. As expected, when larger amounts of protein are added to the surface, a larger fraction of the surface is covered, yielding higher surface pressure–area (π-A) values and shifting the curve to the right.

We compared the shape of the curves to determine the optimal amount of protein to use in further experiments. In the 4 nmol sample, the curve began rising almost immediately (reading right to left). Therefore, there was too much protein to observe the complete gas to liquid transition, even with the barriers fully open. In contrast, the data from 1 nmol of EGFP-Ubx revealed a large (flat) gas phase and the gas-liquid transition, but only a small portion of the curve represented the liquid phase, hampering data analysis. Furthermore, film was not visible by eye, and fibers could not be reliably drawn from the compressed surface. The curve representing 2 nmol of EGFP-Ubx revealed a complete gas-liquid phase transition and a useful amount of data was present in both the liquid and gas phases of the curve. Thus, all further Langmuir experiments used 2 nmol protein.

Table 1. Comparison of limiting areas for Ubx films obtained from 2 nmol EGFP-Ubx using a Langmuir apparatus with different incubation times and subphases.

	Water	**100 mM NaCl**			**100 mM NaCl + 50 mM NaH_2PO_4**			
Time (min)	10	10	60	120	10	30	60	120
LA (cm^2)	128 ± 1	271 ± 2	209 ± 3	417 ± 4	416 ± 7	296 ± 5	456 ± 6	503 ± 5

Data was analysed by calculating the limiting area (LA) from Langmuir-Blodgett curves as the x-axis intercept of the liquid phase portion of the curve[27-30]. The higher the number, the larger the area occupied by the film, and the greater the yield of materials. Importantly, the LA is linearly dependent on the amount of protein added (Figure 4A, inset). This relationship demonstrates that the data is reproducible, and that there are no concentration-dependent processes (e.g. adhesion to the trough) that could confound interpretation of the results.

By using the Langmuir technique to assess early stages of assembly, we are restricted to a subphase with a low saline content. However, altering the salinity has the potential to impact the behavior and stability of proteins, especially proteins, like Ubx, with a high density of charged residues. The amino acid sequence of Ubx includes a 60-amino acid homeodomain (Supplemental Figure 1), which has a predicted net charge of +11. This portion of the protein requires counterions to prevent charge repulsion from disrupting the

protein's structure, leading to aggregation. Prior studies demonstrate that Ubx solubility is indeed sensitive to salt concentration: While Ubx is soluble in a low salt buffer like 20 mM Tris, 100 mM KCl, halving or removing the KCl from this buffer causes some Ubx aggregation[45]. However, in prior aggregation studies, Ubx was mixed into these low salt buffers, instead of being dissolved in a high salt buffer and then applied to the surface of a low salt buffer, as in a Langmuir trough. To examine the effects of the salinity of the subphase, we compared the assembly of 2 nmol of EGFP-Ubx following a 10-minute incubation on the surface of (i) water, (ii) 100 mM NaCl (low saline), or (iii) 100 mM NaCl and 50 mM NaH_2PO_4, pH = 8.0 (buffered low saline) (Figure 1B). Although fusion to EGFP improves Ubx solubility[41], a white precipitate was still observed when using water as the subphase. The loss of a portion of the Ubx molecules to aggregation partially accounts for the small amount of film formed when water was used as a subphase (Figure 4B). Although a visible precipitate did not form when 100 mM NaCl was used as the subphase, less film was formed in saline-only solution than when phosphate buffer was added to the sample. This reduced ability to assemble could be due to loss of protein to micro-aggregation, or to EGFP-Ubx monomers adopting a conformation that was less able to self-assemble.

A critical question is whether Langmuir experiments, using a low salt subphase, can reproduce the same or similar stages of assembly that were observed by SEM (Figure 1)[8]. If the ability of Ubx to assemble, disassemble, and reassemble films is independent or not strongly dependent on salt concentration, then we should be able to reproduce these assembly steps, first observed by electron microscopy, in our Langmuir experiments. If Ubx still undergoes a disassembly step during film formation, we would observe a reduction in the surface area covered by the film - the LA - during the disassembly stage. To search for a disassembly step during film formation on low-salt subphases, we compared the behavior of EGFP-Ubx films as a function of assembly time. The range of selected assembly times spanned those previously established for assembly of Ubx films and fibers (Figure 1)[14].

Our initial experiments used the low saline subphase (100 mM NaCl) (Figure 4C, Table 1). Relative to the 10 minute experiment, the 60 minute surface pressure–area (π-A) isotherm exhibited a large leftward shift, corresponding to a large reduction in film size as measured by LA (at 60 minutes, LA = 209 ± 3 versus 271 ± 2 cm^2 at 10 minutes). This reduction is consistent with the de-polymerization of the randomly organized Ubx film observed by EM (Figure 1), and the irregular surface features of fibers formed by 60 minute films (Figure 2). After a 120 minute incubation, the film has re-grown and exceeds the size of the 10 minute film (LA = 417 ± 4 cm^2). The depolymerization/repolymerization is easily visible on a graph of LA vs polymerization time (Figure 4C inset, Table 1).

If depolymerization is a necessary step in Ubx assembly, then we should also observe a leftward shift of the pressure-area isoform at shorter incubation times in the buffered saline solution. To test this hypothesis, 2 nmol of EGFP-Ubx was added to a buffered subphase (50 mM NaH_2PO_4, 100 mM NaCl pH=8.0) and allowed to incubate for 10, 30, 60, or 120 minutes (Figure 4C, Table 1). Relative to the 10 min isotherm, the 30 minute isotherm also shifted to the left, consistent with the disassembly of random aggregates previously observed by electron microscopy[8]. Likewise, the LA was also reduced from 416 ± 7 cm^2 to 296 ± 5 cm^2. By 60 min incubation the film had regrown to match its initial (10 min) size, with an LA = 433 ± 5 cm^2. The film continued to expand, though at a reduced rate, at longer incubation times, again mimicking observations in high salt conditions. After 120 min incubation, the LA reached 489 ± 3 cm^2. Thus, this assembly behavior is non-monotonic with time.

Importantly, the low salt subphase seems to not only permit formation (and subsequent disassembly) of the random aggregates, but also extends the lifetime of these aggregates. After 60 min incubation, the aggregates formed on 100 mM NaCl are still disassembling (Figure 4D), but have already re-assembled when phosphate buffer is included in the solution (Figure 4C) and in buffers with higher salt concentrations (Figure 1). Given that Ubx first forms random aggregates during self-assembly in both high salt conditions (Figure 1) and low salt conditions (Figure 4), we conclude that the random aggregates are an obligatory step in Ubx assembly.

An unusual feature appeared inconsistently in the surface pressure-area isotherms in several of these experiments. Large bumps were sometimes observed on the right side of the isotherm, before reaching the gas/liquid transition. Examples include the 60 and 120 minute isotherms in Figure 4C and the 10 minute isotherm in Figure 4D. We attribute these bumps to re-orientation of films during compression. As the random aggregates disassemble and re-form using linear protein aggregates, the films become very long and thin. Under surface compression, surface pressure forces the films to rotate such that their narrow axis is parallel to the direction of compression, thus relieving some of the pressure.

3.3 Monomer density and extent of crosslinking

We were surprised that fibers were able to be drawn from films incubated for short periods of time (e.g., 10 min when using a weak saline subphase, Figure 2). The data thus far suggest that these films are composed of random aggregates of Ubx rather than the organized lines of Ubx monomers that

form with longer incubation periods. If the organization of Ubx monomers is different in films using low protein concentrations, a 100 mM NaCl subphase, and short times (condition abbreviated pbt, Table 2) compared to the standard high protein concentration, high salt buffer, and long incubation times (condition abbreviated PBT), then the internal organization of monomers in the resulting fibers should be different as well. These packing differences are expected to alter the interfaces between Ubx monomers within the films and fibers, which, in turn, will impact how the proteins crosslink to stabilize the solid materials.

We used confocal microscopy to compare the amount of Ubx cross-linking in materials formed using different protocols. During materials assembly, Ubx monomer-monomer interactions are reinforced by the spontaneous formation of dityrosine covalent bonds (Figure 5C,D). These dityrosine bonds fluoresce blue (Figure 5A), and contribute to the mechanical strength of the materials[17]. Thus, fibers with the brightest blue fluorescence contain more dityrosine bonds, and are stronger. Many materials exhibit direct links between their structure and their mechanical properties[46,47]. We quantified blue fluorescence to determine whether similar interactions are formed using the two different methods (Fig. 3). Because Ubx films are very thin, it is challenging to reliably quantify fluorescence from dityrosine bonds. Therefore, we created thicker fibers from the Ubx films. Touching a narrow object to the surface of the film causes the film to adhere, lift, and reshape itself into a fiber. To reduce the inner filter effect and allow quantitative measurement of fluorescence on cylindrical fibers, confocal microscopy was used to image a thin slice of intact fibers (Figure 5A).

Because fibers formed using pbt conditions are less organized and more prone to containing gaps and pits, they may appear less fluorescent because these areas lack protein, instead of due to a difference in the arrangement of proteins. By using EGFP-Ubx fusion monomers[16,41] to make the materials, we were able to normalize the intensity of blue fluorescence for the amount green fluorescence provided by EGFP, and thus the amount of protein being imaged. This approach will also normalize the data for differences in fiber size and any expansion or contraction of the fibers caused by the different salt concentrations.

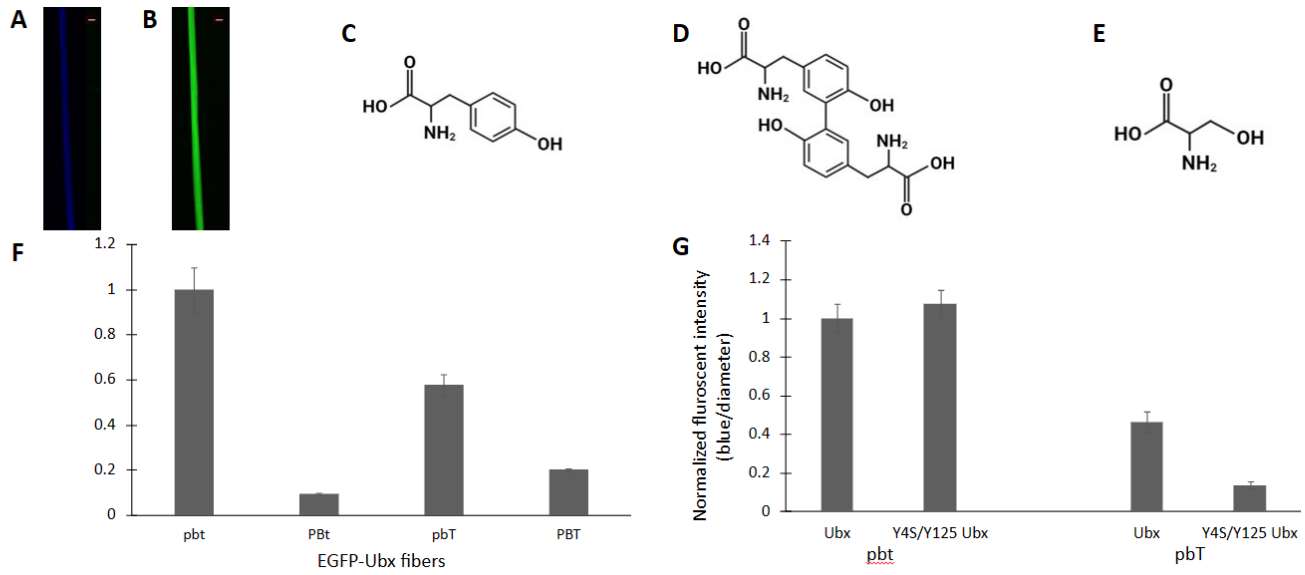

H

Protein	Buffer Used	Time
p: 2 nmol	b: 100 mM NaCl, pH = 7.5	t: 10 minutes
P: 50 nmol	B: 500 mM NaCl + 50 mM NaH_2PO_4 + 5% Glucose, pH = 8	T: overnight

*Figure 5. C*onfocal microscopy of Ubx fibers reveals blue fluorescence of dityrosine bonds (A) and green fluorescence of EGFP (B), in which white scale bars represent 20 µm. Structures of tyrosine (C), dityrosine (D), and serine (E). Normalized fluorescent intensity of EGFP-Ubx fibers for all conditions (F), and for conditions pbt and pbT comparing regular and mutant Ubx fibers. (G) Comparison of the impact of the Y4S/Y12S double mutation on the fluorescence of plain Ubx fibers created from randomly packed films (pbt conditions) and linearly packed films (pbT conditions). (H) Details of conditions used to create fibers for fluorescence experiments.

When fibers are drawn using films assembled in PBT conditions, only six of the fifteen tyrosines in Ubx are able to form tyrosine bonds[17]. This is because the portions of the surface of a Ubx monomer that interface with other monomers are restricted by the ordered arrangement of Ubx monomers into lines during film assembly.

We compared the dityrosine bond content (blue fluorescence / green fluorescence) for fibers made using the conditions identified in this work (designated pbt in Figure 5H) versus previously established conditions (PBT). The blue fluorescence, and therefore the content of dityrosine bonds, was much higher for the pbt fibers than the PBT fibers (Figure 5F). To determine whether incubation time, or protein concentration and subphase composition had the largest impact on dityrosine bond formation, we also made PBt fibers (high amount of EGFP-Ubx used, high salt buffer, short incubation time), and pbT fibers (low EGFP-Ubx used, low salt subphase, long incubation time). While all parameters affected the dityrosine bond content, the protein concentration and subphase composition clearly had the largest effect.

The increased fluorescence of pbt fibers compared to PBT fibers could be due to (i) an increased fraction of Ubx monomers forming the previously discovered dityrosine bonds in the materials, or (ii) the formation of additional, currently unidentified, intramolecular or interdityrosine bonds[18]. To distinguish these possibilities, we compared dityrosine bond formation in fibers formed by a Ubx tyrosine mutant. In PBT conditions, only 6 of the 16 tyrosines in the Ubx sequence are capable of forming dityrosine bonds[17]. In the mutant Y4S/Y12S, the tyrosines (abbreviated Y) at amino acid positions 4 and 12 are mutated to serine (S) (Figure 5E), preventing these positions from forming dityrosine bonds with their obligatory partner amino acids, Y296 and Y293, respectively. If the increased fluorescence of fibers generated using pbt conditions is due to an increased fraction of monomers forming already identified dityrosine bonds, then the Y4S/Y12S Ubx should reduce the fluorescence of materials generated using pbt conditions. However, if this increased fluorescence is due to other bonds forming, these mutations will have little effect on the overall fluorescence.

Based on our Langmuir data (Figure 2), we had hypothesized that under pbT conditions, Ubx was forming films composed of linear arrays of protein, just as it does when assembled using PBT conditions (Figure 1). Indeed, the Y4S/Y12S mutation reduces the fluorescence of fibers formed under pbT conditions, verifying that the films/fibers observed after long periods of time in Figure 2 rely on the same dityrosine bonds as Ubx materials formed under standard, high salt conditions[30]. However, fibers formed using Y4A/Y12S Ubx assembled for short times (pbt conditions) remained as fluorescent as the pbt fibers composed of wild-type Ubx, indicating that the tyrosines at position 4 and 12 are not needed for dityrosine bond formation under these conditions. Therefore, pbt conditions promote the formation of a different set of dityrosine bonds, and organization of monomers in these materials is fundamentally different than in Ubx materials formed under previously established (PBT) conditions.

4. Discussion

With growing advancements in medicine, the need for sophisticated, functionally complex biomaterials has been increasing[48]. Distinct tasks require materials with specific morphologies, mechanical properties, and biological functions. Therefore, generating, varying, and controlling these traits is critical to meeting this need. The most common approach to altering materials is to change the chemical composition of the monomers from which they are formed (e.g., Hedhammar et al., 2010, Howell et al., 2016; Roberts et al, 2020)[17,49,50]. For instance, varying the number and density of elastin motifs in elastin-like peptides allows the creation of microparticles with different complex geometries, such as core-shell, hollow shell, and porous particles[50].

A different approach alters the physico-chemical environment to favor the formation of different monomer-monomer interactions. These altered non-covalent interfaces change the packing of monomers in the materials, altering which covalent cross-links form, and culminating in changing the large-scale structure and properties of the final materials. For example, many smart materials are designed to depolymerize in response to changes in environmental conditions such as pH, temperature, redox status, light, etc[13]. These changes in morphology potentiate the controlled delivery of drugs by triggering loading (materials assembly) and unloading (materials disassembly) conditions. This idea has been extended to transition materials between different, but still assembled, morphologies. For instance, using materials composed of a PDMS/silk bilayer, has developed a strategy to reversibly switch between a smooth and a wrinkled surface using light, temperature and mechanical stretching as stimuli[51].

The environment can also be used to shift either monomer conformation or the preferred monomer-monomer interfaces for assembly, thus driving the formation of different materials using the same monomers. For example, altering the assembly time, temperature or UV-light exposure of supramolecular polymers creates particles of different sizes and topologies[52]. For a recombinant spider silk protein, changing the buffer used for assembly alters tyrosine rigidity and generates fibers with improved mechanical properties[53].

The goal of this study was to create different materials using the same monomers and the same technique, by changing only the assembly conditions. Although many proteins, including Ubx, are capable of forming covalent crosslinks, the initial interactions that drive assembly are non-covalent. Thus, these interactions are also extremely sensitive to the environment. This study was inspired by electron micrographs of early stages of materials assembly, which revealed that Ubx first forms randomly organized aggregates prior to disassembly of that film and repacking Ubx into linear arrays (Figure 1). We discovered that these aggregates are an obligatory intermediate, and that controlling assembly time and buffer composition enables Ubx monomers to create different types of film. These experiments verified the electron microscopy data was not an artifact of sample preparation, and verified that the random Ubx aggregates, once formed, must undergo a disassembly process to create linear protein arrays. Thus, the random aggregates can also be viewed as a kinetic trap on the high-salt assembly pathway. The Langmuir experiments also identified conditions that prolong the longevity of the randomly packed aggregates, allowing them to form films which could be drawn into fibers. These differences in monomer organization cause fibers created from these films to also exhibit different surface structures, wrinkling to different extents. Wrinkles can guide cell topology and cell-materials interactions, and are thus anticipated to be useful applications such as regenerative medicine, drug delivery, and antimicrobial surfaces[32,54,55].

If the organization of monomers is different in these two types of films, we reasoned that their ability to form covalent crosslinks to stabilize and strengthen the resulting materials may also be different. In the linearly organized films formed in high salt, only 6 of the 16 tyrosines in the Ubx amino acid sequence are positioned to form dityrosine covalent bonds. We quantified the extent to which both fibers generated from low-salt or high-salt films were able to fluoresce blue, a hallmark of dityrosine bonds. These experiments demonstrated that the less organized film/fibers actually form more dityrosine bonds. An increase in the number of dityrosine bonds could be due to a greater percentage of Ubx monomers forming the 6 known bonds, or to the alternative packing of Ubx monomers allowing a greater variety of bonds to form. Point mutations removing specific tyrosines (Y4 and Y12) that participate in the formation of known dityrosine bonds dramatically reduced the amount of blue fluorescence in high salt fibers, as expected. However, these mutations had little impact on the fluorescence of materials produced in low salt. Therefore, materials formed using pbt conditions are able to create dityrosine bonds that are inaccessible when assembling in PBT conditions.

5. Conclusion

We have demonstrated that protein assembly conditions can be altered to manipulate monomer-monomer interactions and the organization of monomers within a material, resulting in materials with significantly different properties. Materials formed in low salt conditions exhibit more dityrosine covalent cross-links. Since the mechanical strength of these fibers is generated from dityrosine bonds[15], we would also expect these fibers to be stronger. Furthermore, increased cross-linking is expected to decrease pore size and impact the diffusion of ligands through these materials. Importantly, the activity of a protein (EGFP) genetically fused to Ubx is also preserved during assembly in these low salt conditions. Therefore, this new method does not impede functionalization of these materials via gene fusion. Importantly, the activity of the added protein is preserved and even stabilized in protein materials[16,41,56]. Numerous fusion proteins have been created which incorporate different types of protein activities (e.g. cell binding peptides, cytokines, enzymes and ligand binding proteins)[16,56]. These bioactive materials have the potential to impact in numerous biomedical fields including use in wound healing, drug delivery, tissue engineering, and sensing[57,58].

To fully leverage materials composed of these fusion proteins, the properties of the materials, such as strength and ligand diffusion rate, must match the needs of the intended application. Such properties are most frequently adjusted by either changing the composition of the monomer or by selecting a different method to promote assembly. Importantly, the different materials analysed herein were generated using the same monomers and the same overall assembly technique. We were able to create a variety of materials by altering the chemical environment because Ubx undergoes hierarchical, multi-scale self-assembly in which non-covalent bonds dictate the initial monomer-monomer interactions. This approach to creating new materials does not require new monomers to be designed, and manufactured, nor does it need new equipment or additional experts. Because Ubx shares these traits with many other materials-forming proteins[59,61], we anticipate that altering the assembly conditions could change the structure of many other protein-based materials.

References

1. Lee CH, Singla A and Lee Y (2001) *Int. J. Pharm.* **221** 1

2. Ayoub NA, Garb JE, Tinghitella RM, Collin MA and Hayashi CY 2007 *PLoS One* **2** e514

3. Teulé F, Cooper AR, Furin WA, Bittencourt D, Rech EL, Brooks A and Lewis RV 2009 *Nat. Protoc.* **4** 341

4. Wen H, Lan X, Zhang Y, Zhao T, Wang Y, Kajiura Z and Nakagaki M 2010 *Mol. Biol. Rep.* **37** 1815

5. Champion JA and Pho T 2022 *ACS Appl Mater Interfaces* **14** 51697
6. Nilebäck L, Arola S, Kvivk M, Paananen A, Linder MB and Hedhammar M 2018 *Langmuir* **34**, 11795
7. Bowen CH, Dai B, Sargent CJ, Bai W, Ladiwala P, Feng H, Huang W, Kaplan DL, Galazka JM and Zhang F 2018 *Biomacromolecules* **19** 3853
8. Majithia R, Patterson J, Bondos SE and Meissner KE 2011 *Biomacromolecules* **12** 3629
9. Patterson JL, Arenas-Gamboa AM, Wang TY Hsiao HC, Howell DW, Pellois JP, Rice-Ficht A and Bondos SE 2015 *J. Biomed. Mater. Res. - Part A* **103**, 1546
10. Åstrand C, Chotteau V, Falk A and Hedhammar M 2020 *Biomater. Sci.* **8**, 2514
11. Zhang S, Liu Y, Machatschek R and Lendlein A 2022 *MRS Advances* **7** 56
12. Zhang F, Xie G and Pan J 2017 *Langmuir* **33**, 8749
13. Li Y, Yang G, Gerstweiler L, Than SH and Zhao C-X 2023 *Adv Funct Mater* **33** 2210387
14. Greer AM., Huang Z, Oriakhi A, Lu Y, Lou J and Matthews KS, Bondos SE 2009 *Biomacromolecules* **10** 829
15. Huang Z, Lu Y, Majithia R, Shah J, Meissner K and Matthews KS, Bondos SE, Lou J 2010 *Biomacromolecules* **11** 3644
16. Huang Z, Salim T, Brawley A, Patterson J, Matthews KS and Bondos SE 2011 *Adv. Funct. Mater.* **21** 2633
17. Howell DW, Tsai SP, Churion K, Patterson J, Abbey C, Atkinson JT, Porterpan D, You YH, Meissner KE, Bayless KJ and Bondos SE 2015 *Adv. Funct. Mater.* **25** 5988
18. Patterson JL, Abbey CA, Bayless KJ and Bondos SE 2014 *J. Biomed. Mater. Res. - Part A* **102** 97
19. Patterson JL, Arenas-Gamboa AM, Wang TY, Hsiao HC, Howell DW, Pellois JP, Rice-Ficht A and Bondos SE. *J Biomed Mater Res A* **103** 1546
20. Crawford NF and Leblanc RM 2014 *Adv. Colloid Interface Sci.* **207** 131
21. Hessinger C, Technau GM and Rogulja-Ortmann A. 2017 *Development* **144** 139
22. Nielsen SB Lapierre A, Anderson JU, Pedersen UV and Tomita S, Andersen LH 2001 *Phys. Rev. Lett.* **87** 228102
23. Tsien RY 1998 *Annu. Rev. Biochem.* **67** 509
24. Terauchi Y, Tanaka T, Mitsuishi M, Yabu H, Yoshimi A, Nantani K and Abe K 2020 *Biosci Biotechnol Biochem* **84** 678
25. Hussain SA, Dey B, Bhattacharjee D, Mehta N. 2018 *Heliyon* **4** e01038
26. Pal P, Kamilya T, Mahato M, Talapatra GB 2011 *Surface Rev Lett* **18** 267
27. Estate, B. I. 1990 *Philos. Trans. R. Soc. London. Ser. A, Math. Phys. Sci.* **330** 141
28. Wu Y, Fan H, Yang C and Zhang L 2020 *Colloids Surfaces A Physicochem. Eng. Asp.* **585** 124111
29. Watanabe M, Kosaka Y, Oguchi K, Sanui K and Ogata N 1988 *Macromolecules* **21**, 2997
30. Trillo JM, Jado EI, Fernández SG and Pedrero PS 1972 *Kolloid-Zeitschrift Zeitschrift für Polym.* **250** 325
31. Howell D. Tsai SP, Churion K, Patterson J, Bayless K and Bondos SE 2016 *Biophys. J.* **110** 338a
32. Dimmock RL, Wang X, Fu Y, El Haj AJ and Yang Y 2020 Recent Prog Mater **2** doi:10.21926/rpm.2001005
33. He X and Jiang Y 2017 Substrate curvature regulates cell migration. Phys Biol **14** 035006
34. Li T, Lilja K, Morris RJ and Brandani GB 2019 *J. Colloid Interface Sci.* **540** 420
35. Aveyard R, Clint JH, Nees D and Paunov VN 2000 *Langmuir* **16** 1969
36. Aveyard R, Clint JH, Nees D, Quirke N 2000 *Langmuir* **16** 8820
37. Yeon W-C, Kannan B, Wohland T and Ng V. 2008 *Langmuir* **24** 12142
38. Pegram LM and Record MT. 2007 J Phys Chem B **117** 5411
39. Docoslis A, Giese RF and van Oss CJ 2000 Colloids and Surfaces B: Biointerfaces **19** 147
40. Mendes GG, Booth RM, Pattison DL, Alvarez AJ and Bondos SE 2018 *Methods Enzymol.* **611** 583.
41. Tsai SP, Howell DW, Huang Z, Hsiao HC, Lu Y, Matthews KS, Lou J, Bondos SE. 2015 *Adv Funct Mater* **25** 1442.
42. Langmuir, I. 1917 *J. Am. Chem. Soc.* **39** 1848
43. Langmuir I and Schaefer VJ 1938 *J. Am. Chem. Soc.* 60 1351
44. Blodgett KB 1935 *J. Am. Chem. Soc.* **57** 1007
45. Bondos SE and Bicknell A 2003 *Anal. Biochem.* **16** 223
46. Wegst UGK, Bai H, Saiz E, Tomsia A and Ritchie RO 2015 *Nat. Mater*. **14** 23

47. Grindy SC, Learsch R, Mozhdeli D, Cheng J, Barrett DG, Guan Z, Messersmith PB and Holten-Andersen N 2015 *Nat. Mater.* **14** 1210

48. Huebsch N and Mooney DJ. 2009 *Nature* **462** 426

49. Hedhammar M, Bramfeldt H, Baris T, Widhe M, Askarieh G, Nordling K, von Aulock S and Johansson J 2010 *Biomacromolecules* **11** 953.

50. Roberts S, Miao V, Costa S, Simon J, Kelly G, Shah T, Zauscher S and Chilkoti A. 2020 *Nat Commun* **11** 1342

51. Wang Y, Kim BJ, Peng B, Li W, Wang Y, Li M, and Omenetto FG 2019 Proc Natl Acad Sci U S A. **116** 21361

52. Yagai S, Kitamoto Y, Datta S, and Adhikari B 2019 Acc Chem Res. **52** 1325

53. Stengel D, Saric M, Johnson HR, Schiller T, Diehl J, Chalek K, Onofrei D, Scheibel T and Holland GP 2023 Biomacromolecules. **24** 1463

54. Izawa H, Okuda N, Yonemura T, Kuroda K, Ochi K, Ifuku S, Morimoto M, Saimoto H, Noda M, Azuma K, Okamoto Y, and Ito N 2018 Colloids Interfaces. **2** 15

55. Nguyen DHK, Bazaka O, Bazaka K, Crawford RJ, and Ivanova EP 2020 Trends Biotechnol. **38** 558

56. Howell DW, Duran CL, Tsai SP, Bondos SE, and Bayless KJ 2016 Biomacromolecules. **17** 3558

57. Rosenbloom J, Abrams WR, and Mecham R 1993 FASEB J. **7** 1208

58. Wagenseil JE and Mecham RP 2009 Physiol Rev. **89** 958

59. Revell CK, Jensen OE, Shearer T, Lu Y, Holmes DF, and Kadler KE 2021 Mater Biol. **12** 100079

60. Fan, Li, Cai Z, and Wang X 2021 Nat Commun. **12** 2375

61. Jehele F, Fratzi P, and Harrington MJ 2018 ACS Nano. **12** 2160

Supplemental Information

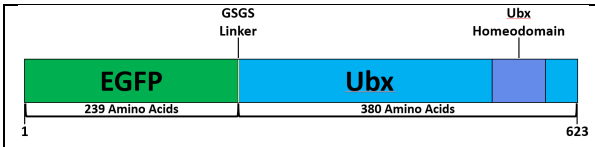

Supplemental Figure 1. Diagram of the EGFP-Ubx fusion sequence. The Ubx1a isoform was used to generate the fusion protein. The positively charged Ubx homeodomain is part of the Ubx amino acid sequence. A four amino acid linker (Gly-Ser-Gly-Ser) was included between the two protein sequences.